Asian Journal of Chemistry; Vol. 27, No. 8 (2015), 2996-3002

ASIAN JOURNAL OF CHEMISTRY

http://dx.doi.org/10.14233/ajchem.2015.18547

Effects of Precipitants on Fischer-Tropsch Synthesis Over Co-Ru-Al_2O_3 Catalysts

YAN LIU[1], LITAO JIA[1], YACHUN LIU[1,2], BO HOU[1] and DEBAO LI[1,*]

[1]Institute of Coal Chemistry, Chinese Academy of Sciences, Taiyuan 030001, Shanxi Province, P.R. China
[2]National and Local United Engineering Laboratory for New Petrochemical Materials and Fine Utilization of Resources, Hunan Normal University, Changsha 410081, P.R. China

*Corresponding author: Tel/Fax: +86 351 4121793; E-mail: dbli@sxicc.ac.cn

Received: 1 August 2014; *Accepted*: 9 December 2014; *Published online*: 27 April 2015; AJC-17180

In this work, the effects of precipitants on the physicochemical properties of the precursors, alumina, catalysts and the corresponding catalytic performance for Fischer-Tropsch synthesis were investigated systematically. Furthermore, the relations between pores size distribution of alumina, cobalt particle sizes and catalytic performance for Fischer-Tropsch synthesis were studied thoroughly. It was found that Boehmite (γ-AlOOH) could be prepared by using ammonia or ammonium bicarbonate as precipitants, respectively, while the ammonium aluminium carbonate hydroxide (AACH) could be prepared from precipitating ammonium carbonate. Different alumina were obtained by roasting the prepared γ-AlOOH and AACH, respectively. The pores size distribution of alumina were tuned by different precipitants and thus the cobalt particle sizes and the reduction behaviours of catalysts supported on the corresponding alumina could be regulated simultaneously.

Keywords: Cobalt, Alumina, Pore size, Particle, Fischer-Tropsch synthesis.

INTRODUCTION

Cobalt-based catalyst is a very competitive system for Fischer-Tropsch synthesis due to its high activity, selectivity of linear hydrocarbon and low activity of methane and water-gas shift reaction[1]. The carrier used plays an important role in designing an efficient cobalt-based Fischer-Tropsch synthesis catalyst. The principal function of carrier is to disperse cobalt and to produce a certain size of cobalt crystal after activation and reduction. The catalytic performance for Fischer-Tropsch synthesis is dependent on the cobalt particle size.

In general, the active phase of cobalt-based catalyst for Fischer-Tropsch synthesis is Co^0 obtained from reducing Co_3O_4. It was found that cobalt particle size had a strong impact on products selectivity[2], C_5^+ selectivity decreased when cobalt metal particles was smaller than 6-8 nm, while the turnover frequency (TOF) for CO hydrogenation was independent of cobalt particle size for catalysts with sizes larger than 6-8 nm[2]. Lermontov *et al.*[3] found that Fischer-Tropsch synthesis reaction rate was proportional to the number of cobalt surface sites for larger cobalt particles, while the specific catalytic activity of these sites was much lower than it could be predicted based on the measurements of cobalt surface sites, when the particles were smaller than 7 nm. Borg *et al.*[4] found that the selectivity of C_5^+ increased sharply with increasing cobalt particle size up to about 7 nm, there was an apparent optimum particle size at approximately 8 nm for the selectivity of C_5^+ and the selectivity was constant for particles larger than 9-10 nm. Borg *et al.*[4] plotted two volcano-like curves that individual propene and propane selectivity was a function of the cobalt particle size. In another study[5], it was reported that chemical reaction of small cobalt particle with the support may result in diffusion of cobalt active phase into alumina and formation of stoichiometric or nonstoichiometric cobalt aluminate spinel, which was inactive for Fischer-Tropsch synthesis. Therefore, effective control of cobalt particle size is very important in developing an cobalt-based catalyst with an excellent Fischer-Tropsch catalytic performance.

Porous structure of the carrier could control the sizes of supported cobalt particles. Khodakov *et al.*[6,7] showed that the sizes of Co_3O_4 crystallites increased with increasing the pore diameter of the silicas used. Similar results[8] about effects of pore sizes on cobalt dispersion and particle sizes for alumina supported cobalt catalysts were also obtained by Holmen and coworkers. Khodakov *et al.*[6] considered that the catalysts supported on the narrow pore size carriers had much lower activity than the counterparts with larger pore sizes. It was considered that lower reducibility of small cobalt particles supported on supports with narrow pores was responsible for the poor catalytic performance.

Alumina is one of the most common commercial carriers applied in Fischer-Tropsch synthesis for its excellent thermal stability, high mechanical resistance, large surface area and pore size[9]. Alumina can be obtained by various processes such as precipitation, sol-gel, hydrothermal, gas phase deposition and combustion ways[10]. Among them, the precipitation method is the most widely used and cost-effective process for preparing alumina. High-grade alumina can be acquired by roasting γ-AlOOH or ammonium aluminium carbonate hydroxide (AACH) produced from precipitation process[11,12]. The chemical composition and textural properties of precursors have dramatic effects on the properties of the resultant alumina[13,14]. It is reported that the composition of precursors prepared by precipitation method are changed with the precipitants used, AACH with various textural properties can be obtained by using such precipitants as ammonia bicarbonate[15] or urea[16], whereas γ-AlOOH can be prepared by using ammonia[17], ammonia bicarbonate[18], ammonia carbonate or sodium carbonate[10] as precipitants.

Alumina with various pore properties can be acquired by roasting various aluminium precursors prepared from different precipitants[10,15-18], however, the Fischer-Tropsch synthesis catalytic performance of cobalt-based catalysts supported on these carriers were less investigated by researchers. Moreover, there are no reports about clarifying the relations of the textural properties of alumina prepared from different precipitants, the supported cobalt particle sizes and the corresponding catalytic performance for Fischer-Tropsch synthesis.

In this work, alumina were prepared by using different precipitants. The chemical composition of aluminium precursors and the physical property of alumina were characterized by XRD, FTIR, SEM, TEM and BET. The 20 % Co-0.1 % Ru-Al_2O_3 catalysts were obtained by impregnating cobalt and ruthenium precursors in the alumina. The pore size distribution of alumina were tuned by using different precipitants. The relations between pore properties of alumina, cobalt particle sizes and catalytic performance for Fischer-Tropsch synthesis were studied thoroughly.

EXPERIMENTAL

Catalysts preparation: About 0.5 mol/L aqueous solution of $Al(NO_3)_3 \cdot 9H_2O$ as aluminium salt and about 1.5 mol/L aqueous solution of ammonia, 1.5 mol/L aqueous solution of ammonium bicarbonate and 1 mol/L aqueous solution of ammonium carbonate as alkaline precipitants, respectively. Precipitation was conducted at a water bath of 60 °C under a stirring speed of 400 rpm by co-precipitation. The precipitation was terminated after 1 h, then, the water bath was heated up to 80 °C and kept for 1 h, finally, the precipitate was washed and filtrated twice by twofold deionized water of suspension, the filter mass was dried at 110 °C for 12 h, then the precursor was obtained. The carriers Al_2O_3 were obtained by roasting the corresponding precursors at 500 °C for 4 h under ambient atmosphere. The 20 % Co-0.1 % Ru-Al_2O_3 catalysts were obtained by introducing $Co(NO_3)_2 \cdot 6H_2O$ and ruthenium(III) nitrosyl nitrate solution in Al_2O_3 by incipient wetness impregnation and drying at 110 °C for 12 h, then roasting at 350 °C for 4 h under air atmosphere. The precursors were denominated as P-A, P-AB and P-AC, respectively. Among them, P stands for precursor, A stands for ammonia, AB stands for ammonium bicarbonate and AC stands for ammonium carbonate. According this rule, the corresponding carriers alumina were denominated as C-A, C-AB and C-AC and the corresponding catalysts were denominated as Cat-A, Cat-AB and Cat-AC, respectively.

The BET surface areas of the prepared catalysts were measured with a Micromeritics model ASAP 2000. The XRD (X-ray diffraction) patterns were recorded on a DX-2700 diffraction meter. The SEM (scanning electronic micrographs) were obtained on LEO 1530 VP. The TEM (transmission electron microscopy) images were recorded using a JEOL-2010 microscope operated. The FTIR (KBr-IR spectroscopy) spectra were recorded in Shimadzu FT25 spectrometer. The TGA (thermogravimetric analyses) was carried out on a TGA-92.

Catalyst tests: The as-prepared catalysts were smashed and sieved to obtain 60-80 mesh. 2 mL of catalysts were evaluated in a stainless-steel fixed-bed reactor (I.D. = 10 mm). After reduction at 400 °C for 6 h and cooling to room temperature, syngas with a H_2/CO mole ratio of 2.0 was switched. Wax and liquid products were collected by hot trap and cold trap, respectively. The exhaust gases were analyzed using carbosieve-packed column with thermal conductivity detector (TCD) and Porapack-Q column with flame ionization detector (FID). Oil and wax were analyzed in a GC-920 chromatograph which was equipped with a 35 m OV-101 capillary column and FID. N_2 with a volume ratio of 4 % was blended in the syn-gas as an internal standard. To ensure reliability of the data, the results weren't be collected until the time on stream (TOS) is 48 h and the nitrogen balance is ensured to be in the range of 100 ± 5 %.

RESULTS AND DISCUSSION

Phase, structure and morphology of precursors: Precipitants have important impacts on the composition of precursors and structure of crystals[10,18]. In this work, ammonia, ammonia bicarbonate and ammonia carbonate were employed as precipitants, respectively. To get pure precipitates, the usage of precipitants follow the proportion in eqns. 1-3. The XRD patterns of precursors prepared by three precipitants are included in Fig. 1. As shown in Fig. 1, different diffraction patterns are obtained by different precipitants. γ-AlOOH (JCPDS card No. 21-1307, 2θ = 14.4°, 28.2°, 38.3°, 49.2°, 55.2°, 64°, 71.9°11) was obtained by using ammonia or ammonia bicarbonate as precipitants (eqns. 4-6 and 7-10), respectively). The diffraction-peak strength of P-A is stronger than that of P-AB. AACH ($NH_4Al(OH)_2CO_3$, JCPDS card No. 42-0250, 2θ = 15.2°, 21.8°, 26.9°, 30.7°, 34.9°, 41°, 52.8°, 55.3°15,16) was obtained by using ammonia carbonate as precipitant (as shown in eqn. 11-16).

$$Al^{3+} + 3NH_3 \cdot H_2O \longrightarrow AlOOH\downarrow + 3NH_4^+ + H_2O \quad (1)$$

$$Al^{3+} + 3NH_4HCO_3 \longrightarrow AlOOH\downarrow + 3NH_4^+ + 3CO_2\uparrow + H_2O \quad (2)$$

$$Al^{3+} + 2(NH_4)_2CO_3 + H_2O \longrightarrow NH_4Al(OH)_2CO_3\downarrow + 3NH_4^+ + CO_2\uparrow \quad (3)$$

$$3NH_3 \cdot H_2O \longrightarrow 3NH_4^+ + 3OH^- \quad (4)$$

$$Al^{3+} + 3OH^- \longrightarrow Al(OH)_3\downarrow \quad (5)$$

$$Al(OH)_3 \longrightarrow AlOOH + H_2O \quad (6)$$

$$3NH_4HCO_3 + 3H_2O \longrightarrow 3NH_4^+ + 3OH^- + 3H_2CO_3 \quad (7)$$

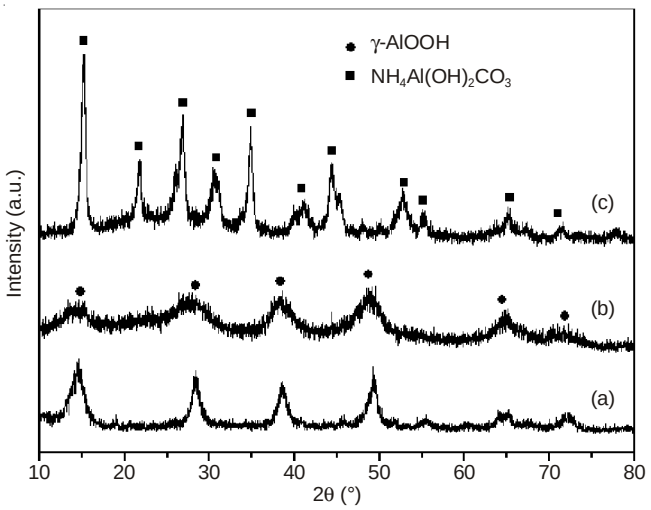

Fig. 1. XRD patterns of precursors: (a) P-A; (b) P-AB; (c) P-AC

$$Al^{3+} + 3OH^- \longrightarrow Al(OH)_3\downarrow \quad (8)$$
$$Al(OH)_3 \longrightarrow AlOOH + H_2O \quad (9)$$
$$3H_2CO_3 \longrightarrow 3CO_2\uparrow + 3H_2O \quad (10)$$
$$2(NH_4)_2CO_3 + 2H_2O \longrightarrow 2NH_4^+ + 2OH^- + 2NH_4HCO_3 \quad (11)$$
$$NH_4HCO_3 + H_2O = NH_4^+ + OH^- + H_2CO_3 \quad (12)$$
$$Al^{3+} + 3OH^- \longrightarrow Al(OH)_3\downarrow \quad (13)$$
$$Al(OH)_3 = AlOOH\downarrow + H_2O \quad (14)$$
$$AlOOH + NH_4HCO_3 \longrightarrow NH_4Al(OH)_2CO_3\downarrow \quad (15)$$
$$H_2CO_3 = CO_2\uparrow + H_2O \quad (16)$$

In order to demonstrate the composition of precursors from another perspective, TG/DTA curves were obtained and displayed in Fig. 2. The weight loss of the precursor is a function of temperature. Precursors P-A and P-AB exhibited weight loss in the temperature range of 100-400 °C, which was attributed to the dehydroxylation of γ-AlOOH and the decomposition was complete at 400 °C around in the present case. The result was coincident with literatures[13,19], while it was reported that the dehydroxylation of γ-AlOOH occurred at 280 °C around and terminated at 500 °C in another literature[17]. The maximum rate of water removal for P-A occurred at about 200 °C, which was higher than the temperature for P-AB of 160 °C, which may be the reason that the crystallinity of P-AB was less integrated compared with P-A. P-AC had a high crystallinity and exhibited sharp endothermic peak at temperature of 200 °C. This peak was attributed to the removal of the volatile species such as carbonates, hydroxides, ammonia and water vapors, which was close to the result of literature[12].

The TG curves agreed with DTA curves, which reveal the same information about the decomposition of precursors. Based on the analysis of TG curves (B) in Fig. 2(a) and 2(b), the total weight loss of P-A amounts to about 25 % and the total weight loss of P-AB is about 24 % for its lower crystallinity. The results are closed to calculated values (26.3 % and 25.4) based on the experimental data, while inconsistent with the theory value (15 %) according to eqn. 17. It is speculated that the prepared γ-AlOOH should contain crystalline water and the decomposition process should be conducted according to the eqn. 18, in which the value of n is about 0.44. The total weight loss of P-AC is about 60 % according to the curve (B) in Fig. 2(c), which is lower than the theoretical value (63.3 %) according to equation (19). However, the theoretical value is nearly coincident with the calculated result (62.6 %) based on the experiment data.

$$2AlOOH \longrightarrow Al_2O_3 + H_2O \quad (17)$$
$$2AlOOH{\cdot}nH_2O \longrightarrow Al_2O_3 + (1 + 2n)\,H_2O \quad (18)\ (n = 0\text{-}1)$$
$$2NH_4Al(OH)_2CO_3 \longrightarrow Al_2O_3 + 2NH_3\uparrow + 2CO_2\uparrow + 3H_2O \quad (19)$$

The composition and crystal structure of the precursors can be better understood with the help of the FTIR characterization. The different absorption bands ascribed to hydroxide, ammonia, carbonate groups and metal-oxygen bonds emerge in Fig. 3. The broad absorption bands around 3443 and 1640 cm^{-1} are assigned to stretching and bending mode of adsorbed water[10]. The bands emerging at 3306, 3094, 1070 and 1160 cm^{-1} in P-A belong to the asymmetric stretching vibration of (Al) O-H, symmetric stretching vibration of (Al) O-H, symmetric deformation vibration of Al-O-H and asymmetric deformation vibration of Al-O-H vibrations of γ-AlOOH, respectively[11,20], which indicate a completed crystal formed in the precursor P-A, while the corresponding bands in P-AB are not intensive owing to its low crystallinity, which is consistent with the analysis result of XRD. The intensive band at 1384 cm^{-1} of P-AB is attributed to the asymmetric bending modes of the residual NH_4^+, which was difficult to wash clean for its glutinous precipitate. There are obvious vibrations of OH^- (ν_{OH} at 3443 cm^{-1}, δ_{OH} at 982 cm^{-1})[19], NH_4^+(ν_{NH} at 3171, 2898 and 2846 cm^{-1}, δ_{NH} at 1826 and 1718 cm^{-1})[16] and CO_3^{2-}(ν_3 at 1554, 1452 cm^{-1} and ν_1 at 1101 cm^{-1}, ν_2 at 848 cm^{-1} and ν_4 at 750 cm^{-1})[17] in P-AC, which clearly indicate that AACH is formed in the P-AC. The bands at 621, 636 and 739 cm^{-1} are ascribed to the vibrational modes of Al-O.

The SEM images of the prepared precursors are shown in Fig. 4. It is reported that the morphology of γ-AlOOH is

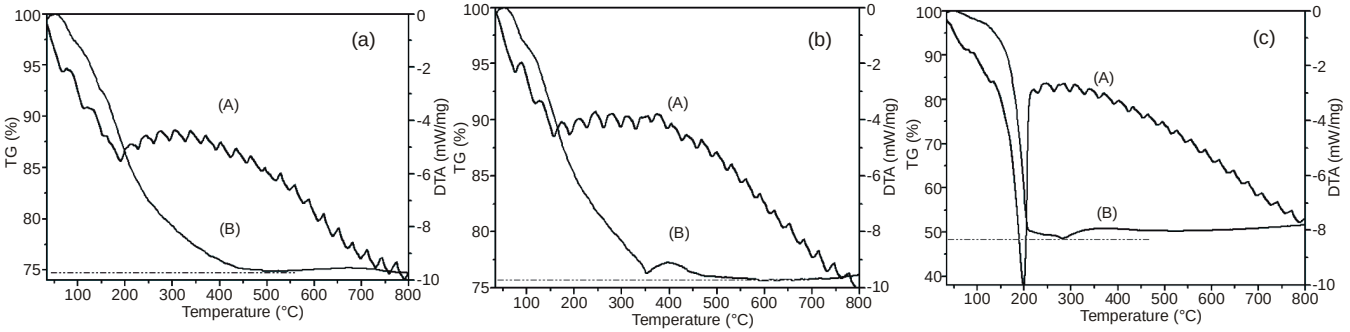

Fig. 2. TG-DTA curves of precursors: (a) P-A; (b) P-AB; (c) P-AC; (A) DTA curve; (B) TG curve

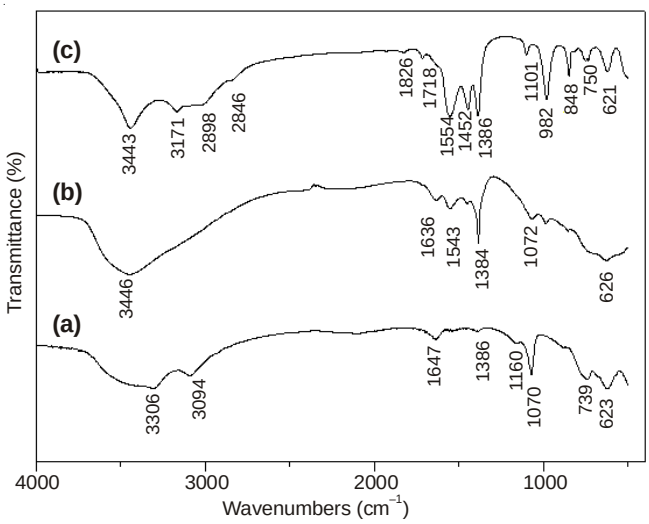

Fig. 3. FTIR spectra of precursors: (a) P-A; (b) P-AB; (c) P-AC

diverse, such as flat plate, flower-like[11], lamellar[20] *etc*. In this study, it is found that P-A appears as spherical, but the spheres are agglomerated each other and the diameter of the sphere is about 20 nm, which is analogous with the results of literatures[13,19]. Meanwhile, the morphology of P-AB is also spherical and the diameter of the spherical is also about 20 nm. Nevertheless, it didn't agglomerate unorderly, but grew up toward one-dimensional rods composing of multi-sphericals. The precursor P-AC is strip with the width of about 30 nm and the length of about 150 nm, similar to the one in some literatures[14,21], while it is reported that AACH were urchin-like[16], lamelliform[15] and cotton-like[12] in other literatures.

Morphology, phase and texture of carriers: Different alumina were obtained by roasting the corresponding precursors at 500 °C for 4 h in air atmosphere and the morphology and microcosmic structure were observed by TEM, as shown in Fig. 5. The morphology of alumina C-A prepared from roasting P-A is granular and about 10 nm size. The crystals are irregular and aggregate each other owing to the aggregated precursor P-A. The morphology of C-AB is similar to C-A, but the crystals are dispersed and some of the crystals grew up toward one-dimensional nano-rods composing of multi-crystals, which is coincident with Ma's result[22]. The morphology of C-AC is strip-shape, which succeeds to the morphology of its precursor and the size is also close to its precursor. Local amplification diagram of C-AC is an inset of Fig. 5(c), it can be observed that there are lots of pores on the surface of C-AC due to abundant NH_3 and CO_2 releasing during the calcinations process (eqn 19). In contrast, there are few pores in the surface of C-A and C-AB for lacking of gas releasing.

The nitrogen adsorption results of the three alumina prepared by different precipitants are listed in Table-1. The alumina C-AC has the highest specific surface area and pore volume for the produced pores *via* releasing CO_2, NH_3 and H_2O during the calcinations process (Fig. 5(c)), while C-A has the smallest specific surface area and pore volume at the same calcinations condition. The difference is attributed to the different decomposition process shown in eqns. 17 and 19, respectively. The pore size distribution curves of alumina prepared by three precipitants are displayed in Fig. 6. C-AC and C-AB display monomodal pore distribution, the most probable pore size of C-AB is 5 nm, which is lower than that of C-AC (12 nm). C-A displays bimodal pore distribution, of which the small pores (5 nm) are attributed to textural-pores, while the big ones (20-70 nm) are attributed to voids enclosed by the disorderly and agglomerate packed sheets[23], thus, C-A display the biggest average pore diameter for its packed pores, as shown in Table-1.

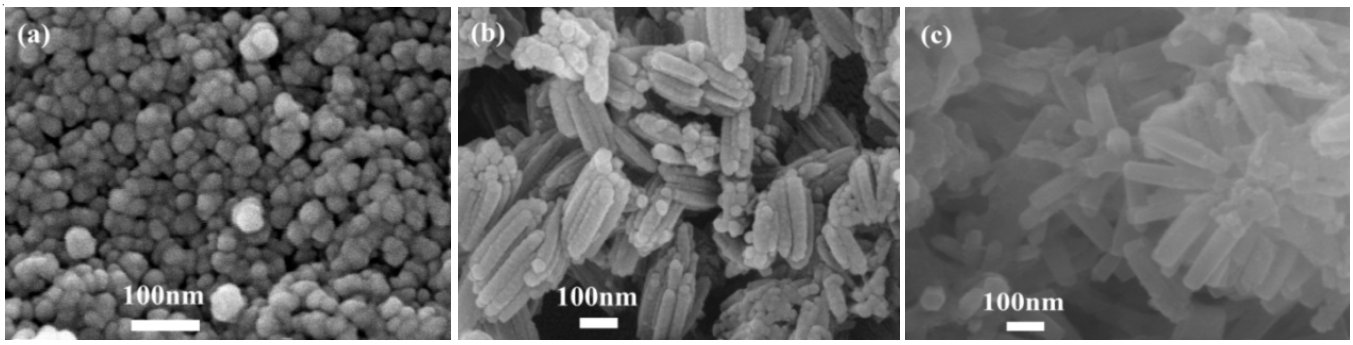

Fig. 4. SEM images of precursors: (a) P-A; (b) P-AB; (c) P-AC

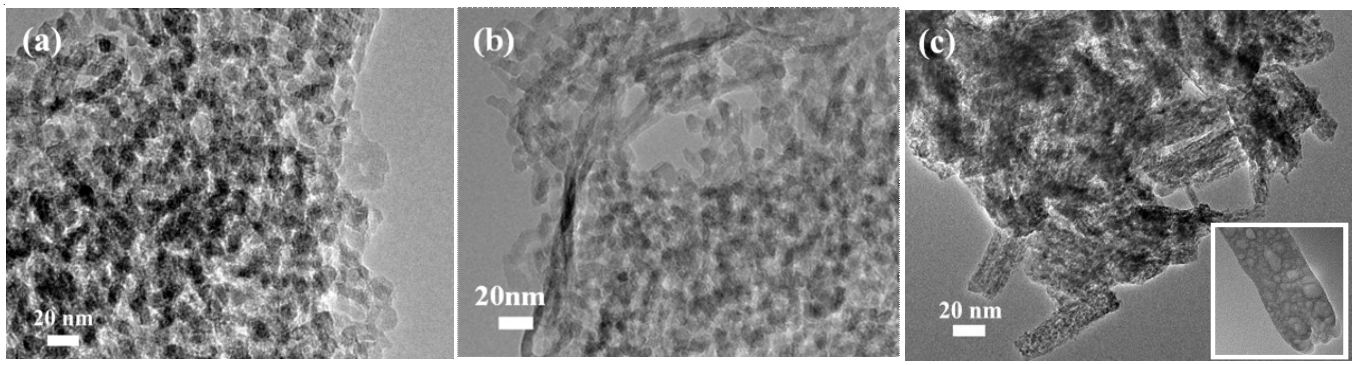

Fig. 5. TEM images of alumina: (a) C-A; (b) C-AB; (c) C-AC

TABLE-1
NITROGEN ADSORPTION RESULTS FOR THE ALUMINA PREPARED BY DIFFERENT PRECIPITANTS

Sample	BET surface area (m^2/g)	Average pore diameter (nm)	Pore volume (m^3/g)
C-A	116	14.2	0.41
C-AB	297	6.4	0.89
C-AC	340	10.6	1.10

TABLE-2
AVERAGE Co_3O_4 CRYSTALS SIZE CALCULATED BY SCHERRER'S FORMULA ($2\theta = 37°$) AND MEASURED FROM TEM

Sample	Crystal size (XRD) (nm)	Average crystal size (TEM) (nm)
Cat-A	14.7	13.9
Cat-AB	6.9	6.8
Cat-AC	10.8	8.7

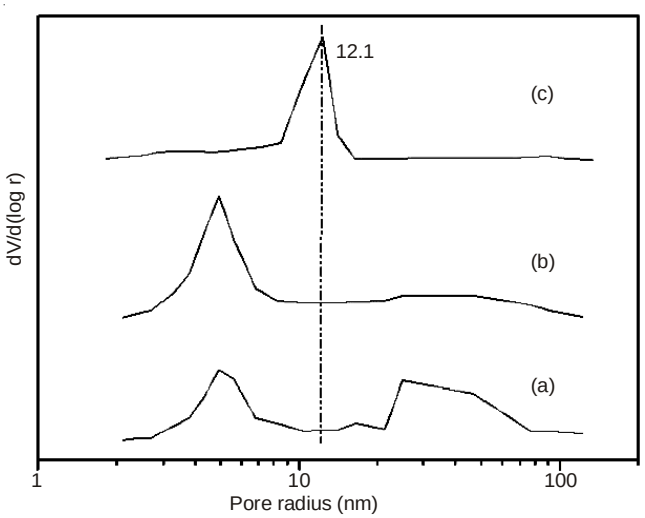

Fig. 6. Pore size distribution of alumina: (a) C-A; (b) C-AB; (c) C-AC

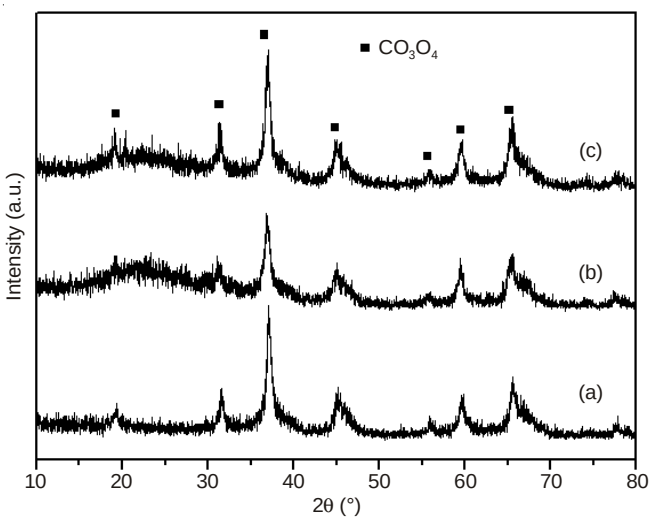

Fig. 8. XRD patterns of Co-Ru-Al_2O_3 catalysts: (a) Cat-A; (b) Cat-AB; (c) Cat-AC

Morphology, crystal phase and reduction behaviour of catalysts: The 20 % Co-0.1 % Ru-Al_2O_3 catalysts were obtained by incipient wetness impregnation of analytical grade $Co(NO_3)_2{\cdot}6H_2O$ and ruthenium(III) nitrosyl nitrate solution in the three alumina, then after drying and calcination. Their TEM images are displayed in Fig. 7 and the corresponding XRD patterns are shown in Fig. 8. Diffraction peaks of Co_3O_4 at the same 2θ of 18.2°, 31.3°, 37°, 45°, 55.8°, 59.4°, 65.2° (JCPDS card No. 43-1003) appears in the three XRD patterns of catalysts. However, the intensity of the three catalysts are not identical, *i.e.* the intensity of catalyst Cat-AB is weaker than the other two and the diffraction peaks of Cat-A were more sharper. The Co_3O_4 particle sizes measured from TEM images and calculated by Scherrer equation at $2\theta = 37°$ are listed in Table-2. The particle sizes of Co_3O_4 were controlled by the pore size of carrier, with small particles formed in narrow pores and large particles formed in wide pores[6-8]. Combined with the curves of pore radius distribution in Fig. 6, C-AB possessed the least pore radius of about 5 nm, leading to the least Co_3O_4 crystal size of 6.9 nm calculated by Scherrer's formula at $2\theta = 37°$, which was close to the average size of 6.8 nm measured from TEM images. The average Co_3O_4 crystal size of Cat-A was 13.9 nm measured by TEM images, which agrees with the size (14.7 nm) calculated by Scherrer's formula. However, it can be seen that both small and big Co_3O_4 crystals existed in Fig. 7(a), for parts of Co^{2+} spilling over from narrow pores and aggregating to generate big Co_3O_4 crystals on the pore mouth. The average crystal size of Cat-AC is 8.7 nm metered from TEM owing to the appropriate carrier pore size, which is smaller than the size of 10.8 nm calculated by Scherrer's formula.

The TPR curves of the three Co-Ru-Al_2O_3 catalysts are shown in Fig. 9. The reduction peaks for Co_3O_4 can be assigned to three-step reduction for catalysts supported on alumina *via* roasting γ-AlOOH or two-step reduction for catalysts supported on alumina *via* roasting AACH, in which the steps

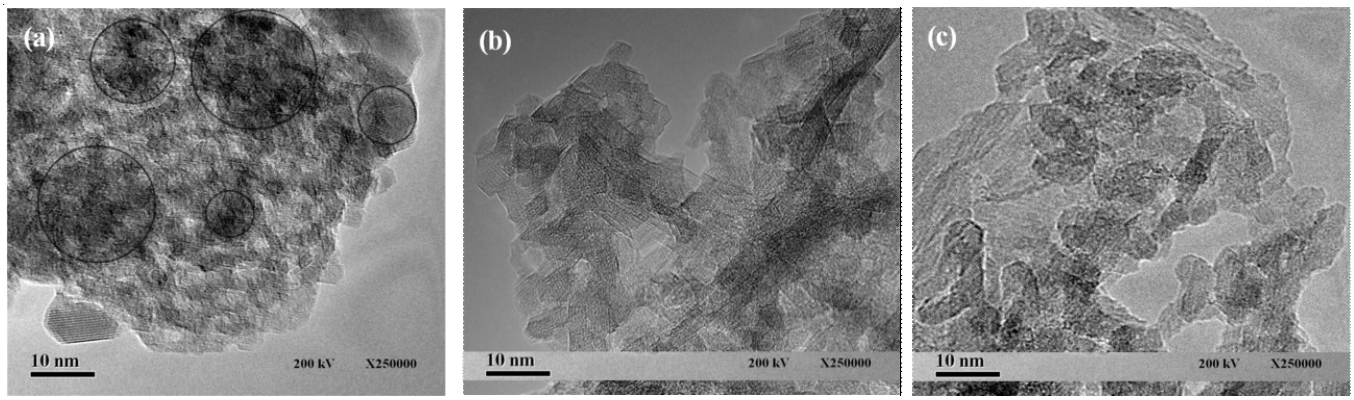

Fig. 7. TEM images of Co-Ru-Al_2O_3 catalysts: (a) Cat-A; (b) Cat-AB; (c) Cat-AC

TABLE-3
CATALYTIC PERFORMANCE OF Co-Ru-Al_2O_3 CATALYSTS FOR FISCHER-TROPSCH SYNTHESIS

Catalysts [a]	CO Conversion (%)	Hydrocarbon distribution (wt. %)			CO_2 selectivity (wt. %)	C_5+ (STY) (g/mL/h)
		CH_4	C_2-C_4	C_5^+		
Cat-A	59.8	17.3	17.8	65.9	2.2	0.07
Cat-AB	77.4	10.5	10.7	78.8	0.3	0.12
Cat-AC	80.9	8.6	8.8	82.6	1.3	0.15

[a]Reaction conditions: 220 °C, 2MPa, GHSV = 1000 h^{-1}, CO/H_2 = 2

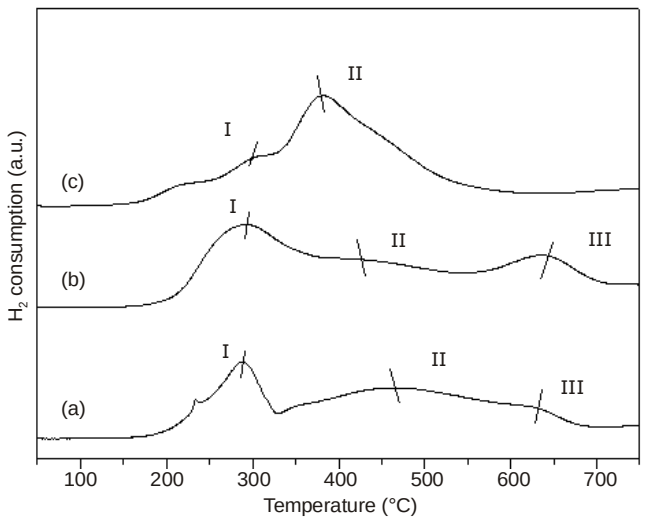

Fig. 9. TPR curves of Co-Ru-Al_2O_3 catalysts: (a) Cat-A; (b) Cat-AB; (c) Cat-AC

can be divided according to the temperature ranges: 200-330, 350-550 and 580-700 °C. The first reduction peak was assigned to the reduction process of transforming Co_3O_4 to CoO, the second peak was assigned to the reduction process of transforming CoO to Co and the third reduction peak was ascribed to the reduction of smaller cobalt crystals, which had strong interaction with the carrier surface and thus generated aluminate which were difficult to be reduced[5,7,22]. The third weak reduction peak only appeared in catalysts supported on alumina (C-A, C-AB) from roasting γ-AlOOH, but not on C-AC from roasting AACH. For the promotion effects of Ru, the reduction temperature of Co-Ru-Al_2O_3 catalysts in this work was lower than the Co-Al_2O_3 catalysts in other study[24,25].

Catalytic performance of catalysts for Fischer-Tropsch synthesis: Fischer-Tropsch synthesis catalytic performance of 20 % Co-0.1 % Ru-Al_2O_3 catalysts prepared by three precipitants are summarized in Table-3. Cat-AC reached the highest CO conversion rate among the three catalysts under the same reaction conditions (220 °C, 2MPa, GHSV = 1000 h^{-1}, CO/H_2 = 2). The CO conversion in the work was higher than that of 25 % Co-0.27 % Ru-Al_2O_3 catalyst1 and was close to that of 30 % Co-0.3 % Ru-Al_2O_3 catalyst in literature[26] under similar reaction conditions. The order of C_5^+ selectivity was Cat-AC > Cat-AB > Cat-A, being same with the order of CO conversion. Combined the data in Table-2, it can be seen that the C_5^+ selectivity was low when the Co_3O_4 particle size was lower than 8 nm, the C_5^+ selectivity reach a peak value when the Co_3O_4 particle size was 8-10 nm and the C_5^+ selectivity again decreased when the Co_3O_4 particle size was bigger than 10 nm, which performed the same law with Borg's research result[4]. The methane selectivity of Cat-AC was only 8.6 % when the CO conversion reached 80.9 %, which was much lower than that of the Co-Al_2O_3 catalysts reported in other literatures[27,28] under similar CO conversion rate. The order of methane selectivity was Cat-AC < Cat-AB < Cat-A, the order of C2-C4 selectivity was also Cat-AC < Cat-AB < Cat-A and the selectivity was near to the value of methane. The methane selectivity decreases with increasing cobalt particle size[2,3], so the methane selectivity of Cat-AC was lower than that of Cat-AB. However, it wasn't suitable for Cat-A due to the aggregated cobalt particles, the reducibility of Cat-A was very low (Fig. 9), resulting to higher methane selectivity. Meanwhile, the produced aluminate in Cat-A was also the major reason for high methane selectivity[7]. To sum up, owing to the big specific surface area, big pore volume and proper pore size for alumina C-AC *via* roasting AACH, the Cat-AC possessed the optimal cobalt particle size, high reducibility and low interaction between cobalt and surface alumina and thus showed higher CO conversion rate, low methane selectivity and higher C_5^+ space-time yield, which was much more excellent than that supported on alumina *via* roasting γ-AlOOH.

Conclusion

γ-AlOOH can be prepared by using ammonia or ammonium bicarbonate as precipitants, while AACH can be prepared by using ammonium carbonate as precipitant. The alumina obtained by roasting AACH possessed the biggest specific surface area of 340 m^2/g, pore volume of 1.1 m^3/g and the average pore radius of 10.6 nm. The cobalt particle size of catalyst supported on this carrier was about 8.7 nm measured by TEM, which benefited to accquire the highest CO conversion of 80.9 % and the lowest CH_4 selectivity of 8.6 % for Fischer-Tropsch synthesis. The performance was much more execllent than that supported on alumina *via* roasting γ-AlOOH, exspecially for the support prepared by ammonia. In conclusion, alumina obtained from roasting AACH would be expected to be a prospective support for the Fischer-Tropsch synthesis cobalt-based catalysts.

ACKNOWLEDGEMENTS

The authors acknowledge the financial support from the National Natural Science Foundation of China (Grant No. 21003149 and 21203232).

REFERENCES

1. W.P. Ma, G. Jacobs, R.A. Keogh, D.B. Bukur and B.H. Davis, *Appl. Catal. A*, **437-438**, 1 (2012).
2. G.L. Bezemer, J.H. Bitter, H.P.C.E. Kuipers, H. Oosterbeek, J.E. Holewijn, X. Xu, F. Kapteijn, A.J. van Dillen and K.P. de Jong, *J. Am. Chem. Soc.*, **128**, 3956 (2006).
3. A.S. Lermontov, J.B. Girardon, A. Griboval-Constant, S. Pietrzyk and A.Y. Khodakov, *Catal. Lett.*, **101**, 117 (2005).

4. O. Borg, P.D.C. Dietzel, A.I. Spjelkavik, E.Z. Tveten, J.C. Walmsley, S. Diplas, S. Eri, A. Holmen and E. Rytter, *J. Catal.*, **259**, 161 (2008).
5. M.R. Hemmati, M. Kazemeini, F. Khorasheh and J. Zarkesh, *J. Taiwan Inst. Chem. Eng*., **44**, 205 (2013).
6. A.Y. Khodakov, A. Griboval-Constant, R. Bechara and V.L. Zholobenko, *J. Catal.*, **206**, 230 (2002).
7. A.Y. Khodakov, J.S. Girardon, A. Griboval-Constant, A.S. Lermontov and P.A. Chernavskii, *Stud. Surf. Sci. Catal.*, **147**, 295 (2004).
8. O. Borg, S. Eri, E. Blekkan, S. Storsater, H. Wigum, E. Rytter and A. Holmen, *J. Catal.*, **248**, 89 (2007).
9. P. Pansanga, J. Panpranot, O. Mekasuwandumrong, C. Satayaprasert, J.G. Goodwin and P. Praserthdam, *Catal. Commun.*, **9**, 207 (2008).
10. D.C. Shin, S.S. Park, J.H. Kim, S.S. Hong, J.M. Park, S.H. Lee, D.S. Kim and G.D. Lee, *J. Ind. Eng. Chem.*, **20**, 1269 (2014).
11. Z. Tang, J.L. Liang, X.H. Li, J.F. Li, H.L. Guo, Y.Q. Liu and C.G. Liu, *J. Solid State Chem.*, **202**, 305 (2013).
12. X.F. Hu, Y.Q. Liu, Z. Tang, G.C. Li, R.Y. Zhao and C.G. Liu, *Mater. Res. Bull.*, **47**, 4271 (2012).
13. J. Kong, B.X. Chao, T. Wang and Y.L. Yan, *Powder Technol.*, **229**, 7 (2012).
14. H. Liu, H.J. Sun, J.Q. Li, X.M. He and Z.F. Zhu, *Adv. Powder Technol.*, **23**, 164 (2012).
15. Z.S. Wu, Y.D. Shen, Y. Dong and J.Q. Jiang, *J. Alloys Comp.*, **467**, 600 (2009).
16. M. Abdullah, M. Mehmood and J. Ahmad, *Ceram. Int.*, **38**, 3741 (2012).
17. X.L. Du, Y.Q. Wang, X.H. Su and J.G. Li, *Powder Technol.*, **192**, 40 (2009).
18. K.M. Parida, A.C. Pradhan, J. Das and N. Sahu, *Mater. Chem. Phys.*, **113**, 244 (2009).
19. H.K. Varma, T.V. Mani, A.D. Damodaran, K.G. Warrier and U. Balachandran, *J. Am. Chem. Soc.*, **77**, 1597 (1994).
20. G.J. Ji, M.M. Li, G.H. Li, G.M. Gao, H.F. Zou, S.C. Gan and X.H. Xu, *Powder Technol.*, **215-216**, 54 (2012).
21. G.C. Li, Y.Q. Liu, L.L. Guan, X.F. Hu and C.G. Liu, *Mater. Res. Bull.*, **47**, 1073 (2012).
22. C.C. Ma, N. Yao, Q. Han and X.N. Li, *Chem. Eng. J.*, **191**, 534 (2012).
23. T.L. Hong, H.T. Liu, C.T. Yeh, S.H. Chen, F.C. Sheu, L.J. Leu and C.I. Wang, *Appl. Catal. A*, **158**, 257 (1997).
24. A.M. Hilmen, D. Schanke, K.F. Hanssen and A. Holmen, *Appl. Catal. A*, **186**, 169 (1999).
25. H.F. Xiong, Y.H. Zhang, K.Y. Liew and J.L. Li, *Fuel Process. Technol.*, **90**, 237 (2009).
26. A. Tavasoli, R.M. Malek Abbaslou and A.K. Dalai, *Appl. Catal. A*, **346**, 58 (2008).
27. H.F. Xiong, Y.H. Zhang, S.G. Wang and J.L. Li, *Catal. Commun.*, **6**, 512 (2005).
28. J.L. Zhang, J.G. Chen, J. Ren and Y.H. Sun, *Appl. Catal. A*, **243**, 121 (2003).